Supplement of Atmos. Chem. Phys., 25, 13279–13297, 2025 https://doi.org/10.5194/acp-25-13279-2025-supplement © Author(s) 2025. CC BY 4.0 License.





Supplement of

Unveiling the formation of atmospheric oxygenated organic molecules under anthropogenic-biogenic interactions: insights from binned positive matrix factorization on multi-subrange mass spectra

Junchao Yin et al.

Correspondence to: Wei Nie (niewei@nju.edu.cn)

The copyright of individual parts of the supplement might differ from the article licence.

1	
2	
3	Supplement
4	••
5	
6	
7	
8	Table of Contents
9	S1 Additional details for the instruments2
10	S2 Related Calculation of OOMs4
11	S3 PMF input and diagnostics for each range6
12	S4 Selected PMF solution for each range8
13	S5 Contributions of factors to total concentration
14	S6 Correlation of binPMF factors with other data
15	S7 Reactivity of nighttime oxidants with BVOCs13
16	S8 Time series of N1-IP factor and C ₅ H ₈ O ₅ N14
17	S9 Dynamic chemical analysis of specific factors
18	S10 Main peaks of binPMF factors

S1 Additional details for the instruments

S1.1 Flow settings of the instruments

- 21 For the CI-APi-TOF measurements, ambient air was drawn into a laminar flow reactor
- 22 through a stainless-steel tube (100 cm long, 3/4 in. diameter) at a flow rate of 10 L/min.
- 23 A sheath flow of 25 L/min of purified airflow was used to maintain laminar flow
- 24 conditions within the reactor. Nitrate reagent ions were generated in the sheath flow by
- 25 exposing air-conditioning nitric acid to a photoionizer X-ray (Model L9491,
- Hamamatsu, Japan). The PTR-MS sampled air at a flow rate of 200 mL/min and was
- 27 connected to an external pump operating at 1.5 L/min to assist in flow control. Flow
- 28 settings and additional details for other instruments used in this study are summarized
- in Table S1.

19

20

30

Table S1. Settings for instrumentations used in this study

Measurement	Instruments	Manufacturer	Sample flow	Resolustion
OOMs	CI-APi-TOF	Aerodyne Research, USA/ Tofwerk AG, Switzerland	10 L/min	30 min/1s
VOCs	PTR-TOF	Ion-icon Analytik, Austria	0.2 L/min	10 min/1min
$PM_{2.5}$	SHARP-5030	Thermo Fisher Scientific, USA	16.7 L/min	5 min
O_3	TEI-49i	Thermo Fisher Scientific, USA	0.7 L/min	5 min/1 min
NO_x	TEI-42i	Thermo Fisher Scientific, USA	1.285 L/min	5 min/1 min
SO_2	TEI-43C	Thermo Fisher Scientific, USA	0.5 L/min	5 min/1 min
СО	TEI-48C	Thermo Fisher Scientific, USA	1 L/min	5 min/1 min

31

32

S1.2 Sulfuric acid calibration and transmission test

- 33 The sulfuric acid calibration factor used in this study was obtained following the
- method described by Kürten et al. (2012), and the results are shown in Fig. S1. The
- 35 transmission efficiency of the CI-APi-TOF as a function of mass was evaluated using
- 36 perfluorinated organic acids, including Propanoic acid, Pentanoic acid, and Heptanoic
- acid. The outcome of the transmission test is also presented in Fig. S1.

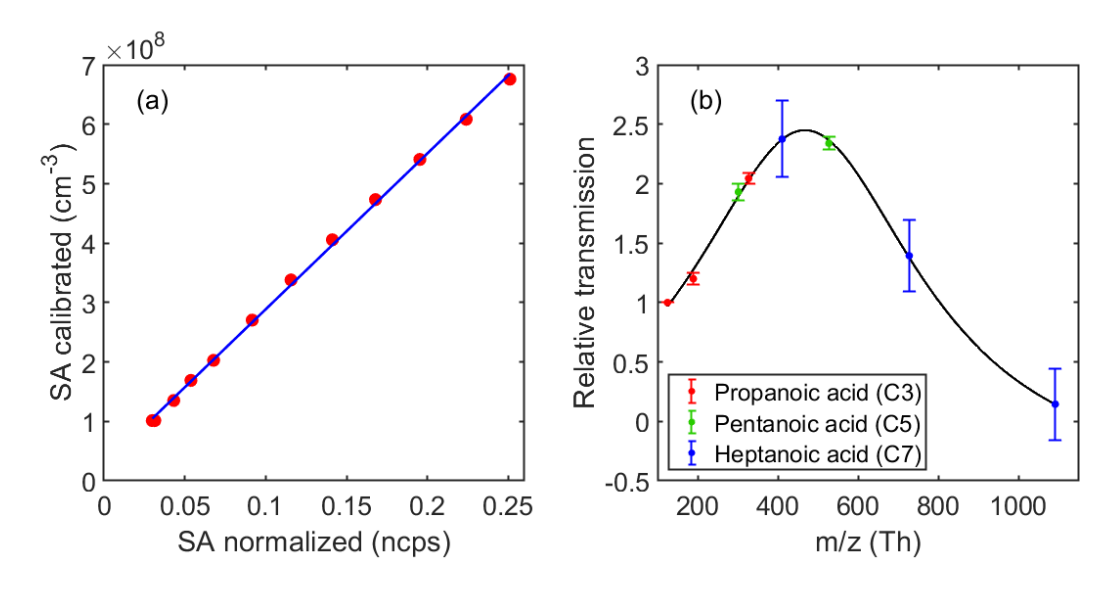


Figure S1. (a) Calibration of sulfuric acid (SA) using the method described by Kürten et al. (2012). (b) Mass-dependent transmission efficiency of the CI-APi-TOF.

S2 Related Calculation of OOMs

- 42 Carbon oxidation state (OSc). The OSc of each non-nitro OOM was calculated based
- on Eq. S1 modified from that in Kroll et al. (2011) include organic nitrate contributions,
- by assuming that all nitrogen come from the nitrate group (-ONO₂).

$$OS_c = \frac{2(n_O - 3n_N)}{n_C} - \frac{n_H}{n_C} + \frac{n_N}{n_C}.$$
 (S1)

46

41

- 47 **Double bond equivalent (DBE).** The DBE of each OOM was calculated using Eq.S2,
- based on the assumption that all nitrogen come from the nitrate group (-ONO₂) or nitro
- 49 group (-NO₂). DBE represents the combined effect of double or triple bonds, as well as
- 50 the ring structure in the molecule, helping to identify the class of precursors of OOM
- 51 (Nie et al., 2022).

$$DBE = n_C + 1 - \frac{n_H + n_N}{2}. (S2)$$

53

- 54 Effective Oxygen Number (noeff). The effective oxygen number was calculated using
- 55 Eq.S3, by assuming that all nitrogen of non-nitro OOM come from the nitrate group (-
- 56 ONO₂):

$$n_{O_{eff}} = n_O - 2 \times n_N. \tag{S3}$$

58

- Volatility Basis Set (VBS). The saturation concentration at 300K of OOMs can be used
- as a characterization of volatility and was calculated using Eq.S4 based on the group-
- 61 contribution method proposed by Donahue et al. (2011):

62
$$log_{10}C^*(300K) = (25 - n_C) \cdot b_C - (n_O - 2n_N) \cdot b_O - 2b_{CO} \left[\frac{(n_O - 2n_N) \cdot n_C}{n_C + n_O - 2n_N} \right]. (S4)$$

63

- 64 where b_C =0.475, b_O =2.3, b_{CO} =-0.3. The effect of nitrate group (-ONO₂) on volatility is
- 65 similar to hydroxyl group (-OH).
- 66 Furthermore, since monoterpene-derived OOMs primarily contain hydroperoxide
- 67 groups (-OOH) and nitrate groups (-ONO₂), their saturation concentrations were
- estimated using methods reported by Mohr et al. (2019):

$$log_{10}C^*(300K) = (25 - n_C) \cdot b_C - (n_O - 3n_N) \cdot b_O$$

$$-2b_{CO} \left[\frac{(n_O - 3n_N) \cdot n_C}{n_C + n_O - 3n_N} \right] - n_N \cdot b_N.$$
(S5)

- where $b_{\rm C}$ =0.475, $b_{\rm O}$ =0.2, $b_{\rm CO}$ =0.9, $b_{\rm N}$ =2.5. In this study, the identification of
- monoterpene-related compounds was based on the approach proposed by Nie et al.
- 73 (2022), where OOMs with DBE=2 that appeared in the PMF monoterpene-related
- 74 factors were classified as monoterpene OOMs.
- 75 The temperature dependence of volatilities is described by Eq.S6, according to
- 76 Stolzenburg et al. (2018):

77
$$log_{10}C_i^*(T) = log_{10}C_i^*(300K) + \frac{\Delta H_{vap}}{R \cdot \ln(10)} \left(\frac{1}{300} - \frac{1}{T}\right)$$
 (S6)

- The evaporation enthalpy (ΔH_{vap}) can be linked to the saturation mass concentration at
- 300K, log₁₀C*(300K), based on Donahue et al. (2011) and combined with Epstein et al.
- 81 (2010):

82
$$\Delta H_{van}[k|mol^{-1}] = 129 - 5.7 \cdot log_{10}C_i^*(300K) \tag{S7}$$

78

- 84 **Hydroxyl radical (OH) estimate.** The concentration of OH radical was calculated by
- applying Eq.S8, based on the assumption that gaseous SA is produced primarily by the
- oxidation of SO₂ by OH and is lost mainly through condensation on particles.

$$[OH] = \frac{[H_2SO_4] \cdot CS}{k_{OH+SO_2} \cdot [SO_2]}.$$
 (S8)

88

- where the constant k_{OH+SO_2} is a termolecular reaction constant for the rate-limiting
- step of the formation pathway of SA in the atmosphere (Finlayson-Pitts and Pitts, 2000).
- The condensation sink (CS) is the loss rate of SA by condensation of the aerosol surface,
- which is calculated by the following Eq. S9 (Kulmala et al., 2012):

$$CS = 2\pi D \sum_{i} \beta_{m_i} d_{p_i} N_i. \tag{S9}$$

94

- where D is the diffusion coefficient of gaseous SA, β_m is a transition-regime correction
- factor dependent on the Knudsen number (Fuchs and Sutugin, 1971), and d_{pi} and N_i are
- 97 the diameter and number concentration of particles in size bin *i*.

S3 PMF input and diagnostics for each range

S3.1 binPMF inputs

Consistent with previous studies employing the binPMF methodology (Liu et al., 2021, 101 2023), the mass spectrometry data were divided into narrow bins with a width of 0.004 102 103 Th after mass axis calibration to construct the input data matrix for PMF analysis. Data quality control measures were implemented by excluding periods of instrumental 104 instability and retaining only signal regions with meaningful signals in the mass spectra 105 between N-0.1 and N+0.4 Th. The three ranges contained 17280, 18105, 18812 bins. 106 The data were averaged into 30 min time resolution, and finally we got 1679 time points 107 in the data matrix. The error matrix was calculated according to Zhang et al. (2019). To 108 109 minimize the potential influence of nitrophenols and fluorinated contaminants on the 110 final PMF results, these compounds were systematically down-weighted in the analysis.

111112

113

114115

116117

118

119

120

121

122

123

124

125

126

127

128

129

130

131

132

133

134

135

136

99

100

S3.2 Diagnosis of binPMF solutions

As established in previous works applying PMF (Ulbrich et al., 2009; Yan et al., 2016), determining the optimal number of factors represents a critical step in the interpretation of PMF results. Accordingly, we systematically evaluated and diagnostically examined solutions encompassing a comprehensive range of factor numbers from 1 to 20 to ensure robust factor resolution. The Q/Q_{exp} ratio exhibited a decreasing trend with increasing factor numbers, albeit with a diminishing rate of reduction (Fig. S1). When the number of PMF factors exceeded eight across all mass ranges, the Q/Q_{exp} ratio stabilized at relatively low levels, accompanied by an explanation ratio exceeding 90% for the original dataset. While higher factor numbers facilitate the resolution of more subtle details within the data, excessive factor decomposition may lead to physically meaningful factors being artificially fragmented into less interpretable ones. In the Range 1, significant influence from nitrophenols was observed. The 10-factor solution successfully isolated and removed the nitrophenol-dominated factors without compromising subsequent analytical interpretations. The N2-MT-I factor was only resolved in the 12-factor solution. Further increasing the number of factors did not yield additional meaningful factors but rather resulted in excessive decomposition of existing factors, thereby compromising the analytical utility of the solution. Consequently, we conducted rotational ambiguity analysis on the 12-factor solution, systematically varying the fpeak parameter from -1 to 1 with an increment of 0.1. Notably, for R1, the fpeak range was extended to 1.5 to identify potentially more optimal solutions. Through this rotational analysis, we selected solutions that maximized the separation between contamination factors and NP-dominated factors. These specifically separated factors were subsequently excluded from further analytical consideration. Similarly, we performed this analytical framework to both R2 and R3, ultimately identifying 11-factor solutions as the optimal configurations for each respective dataset.

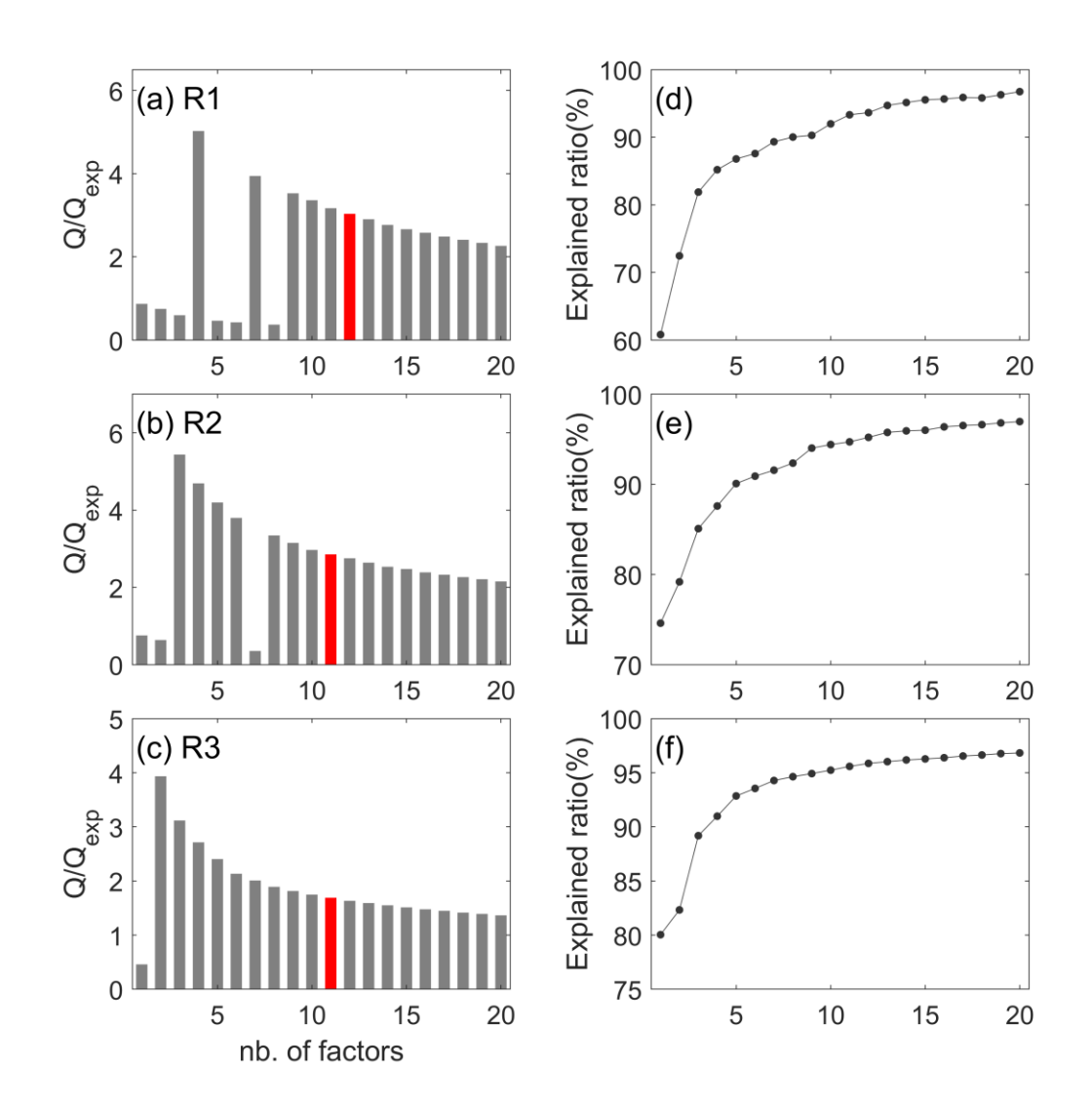


Figure S2. Diagnistics of PMF solutions, including (a)-(c) the variation of $Q/Q_{\rm exp}$ and (d)-(f) explained ratio of PMF factors relative to the number of factors in three range. The red bars indicate the selected PMF solution.

S4 Selected PMF solution for each range

The final PMF solutions selected for each range are presented in Fig. S2-S4. Notably, Range 3 exhibited two closely related factors (D3-AVOC-III-1, D3-AVOC-III-2) that demonstrated strong correlation with corresponding factors in the first two ranges only after factor merging. Therefore, these two factors were consolidated into a single composite factor (D3-AVOC-III) for subsequent analytical interpretation. The merging was performed as follows:

First, the time series of the two factors were summed to create the time series (ts) of the new merged factor. Then, the original time series and profiles of each factor were used to reconstruct their respective data matrices (A1 and A2) by matrix multiplication. These two matrices were then added to obtain the data matrix A of the combined factor:

$$A = A_1 + A_2 = (ts_1 \cdot pr_1) + (ts_2 \cdot pr_2)$$
 (S10)

Finally, the new profile (pr) of the merged factor was derived by solving the equation: $ts \cdot pr = A$ (S11)

This approach preserved both the temporal and spectral information of the original two factors and ensured consistency in subsequent correlation analysis across subranges.

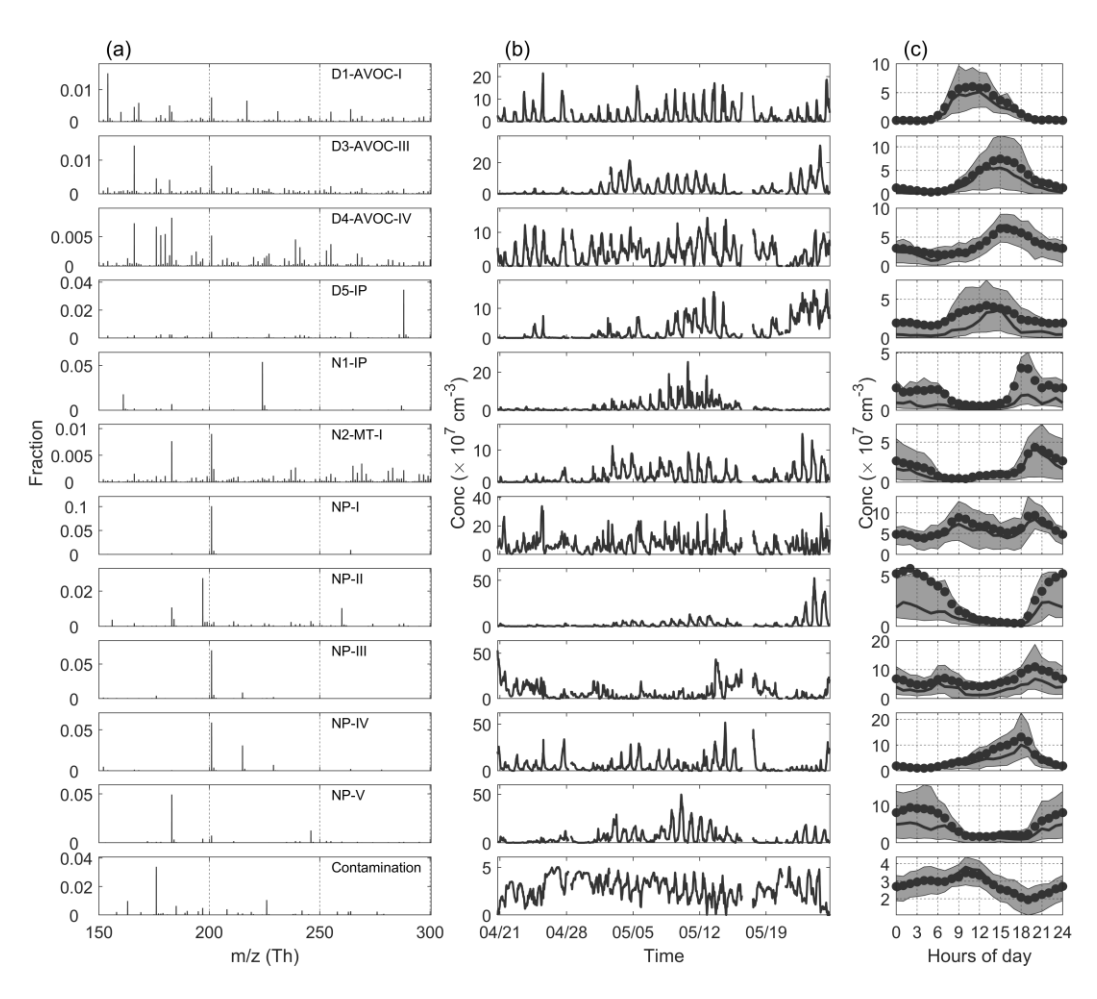


Figure S3. Selected PMF solution for Range 1. (a) PMF factor profiles. (b) Time series of these factors. (c) Diurnal variations in PMF factors.

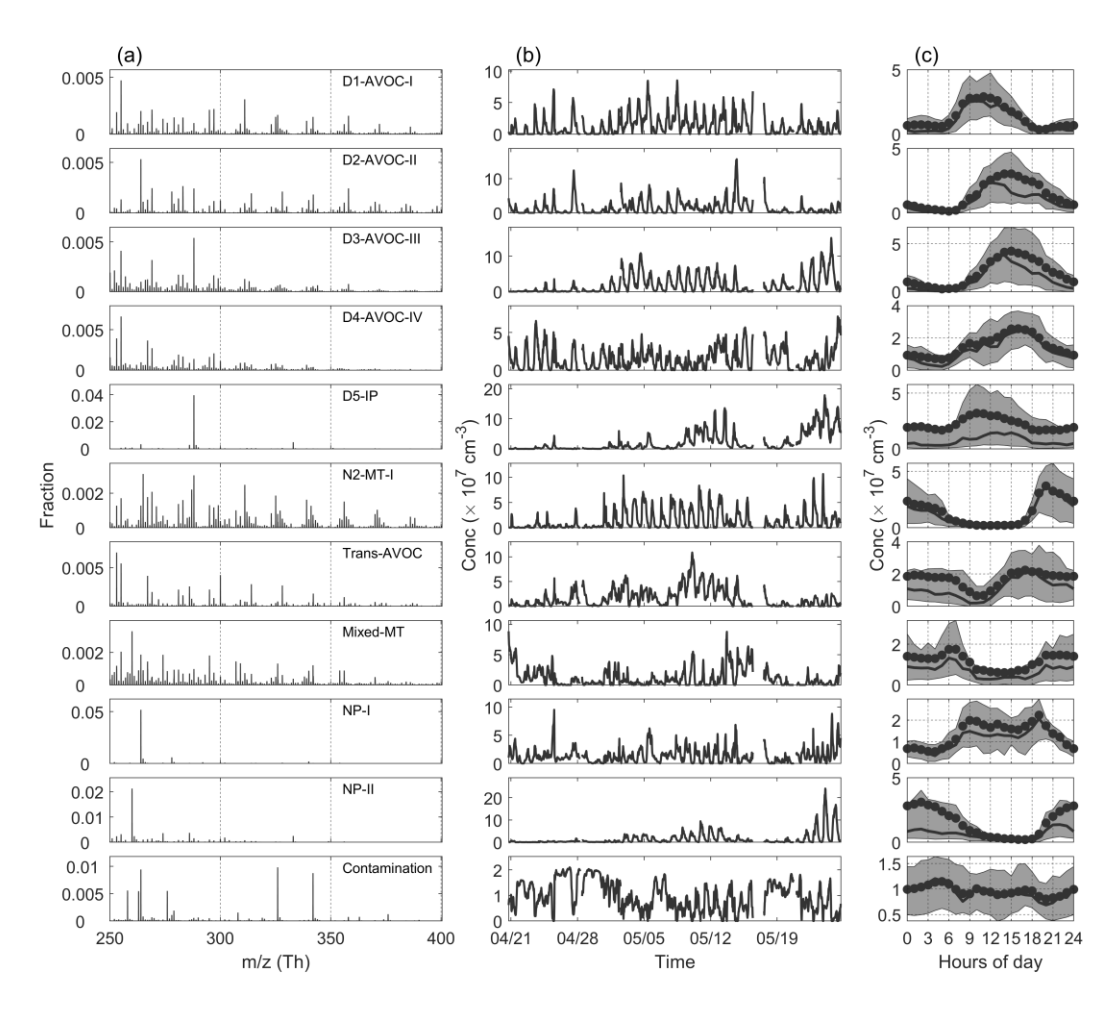


Figure S4. Selected PMF solution for Range 2. (a) PMF factor profiles. (b) Time series of these factors. (c) Diurnal variations in PMF factors.

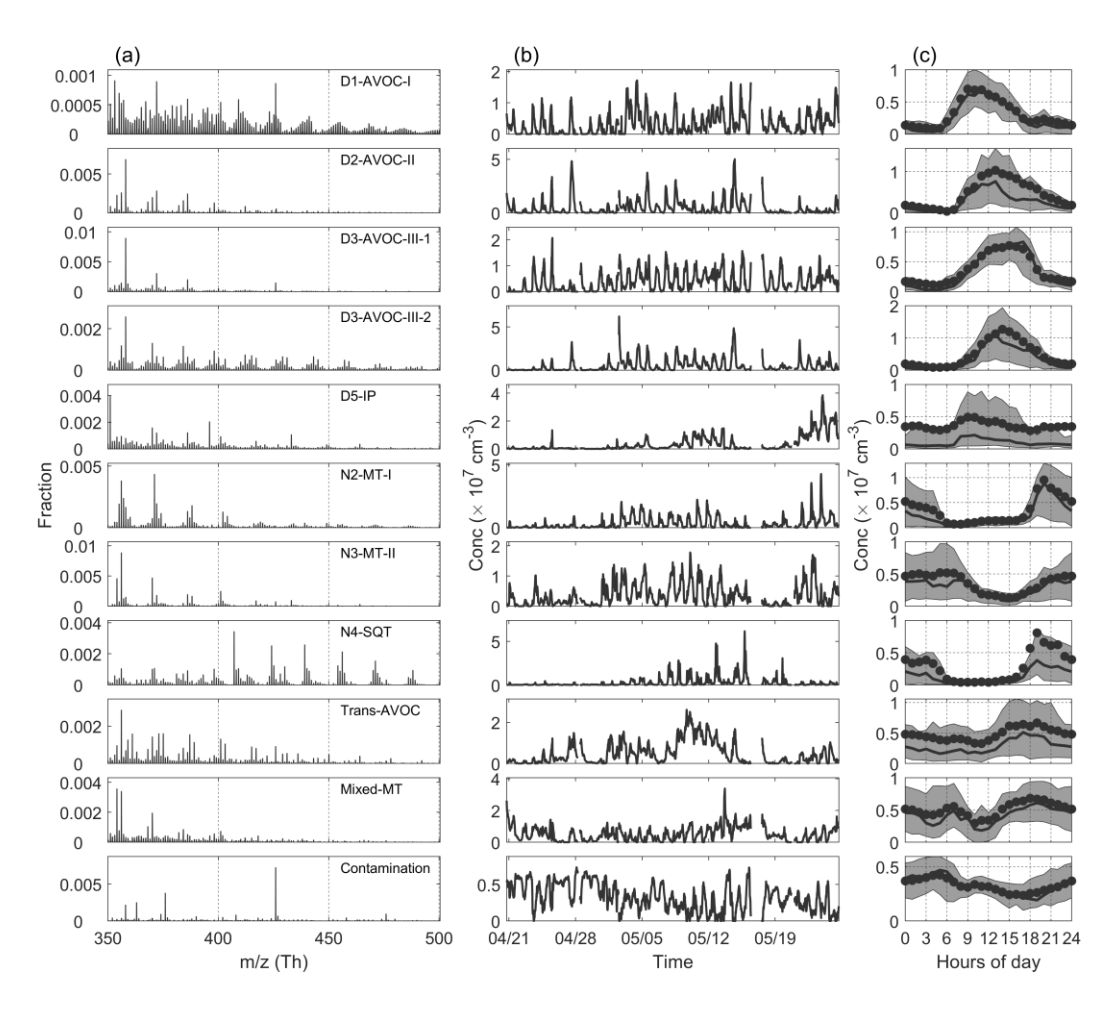


Figure S5. Selected PMF solution for Range 3. (a) PMF factor profiles. (b) Time series of these factors. (c) Diurnal variations in PMF factors.

174 S5 Contributions of factors to total concentration

175

178

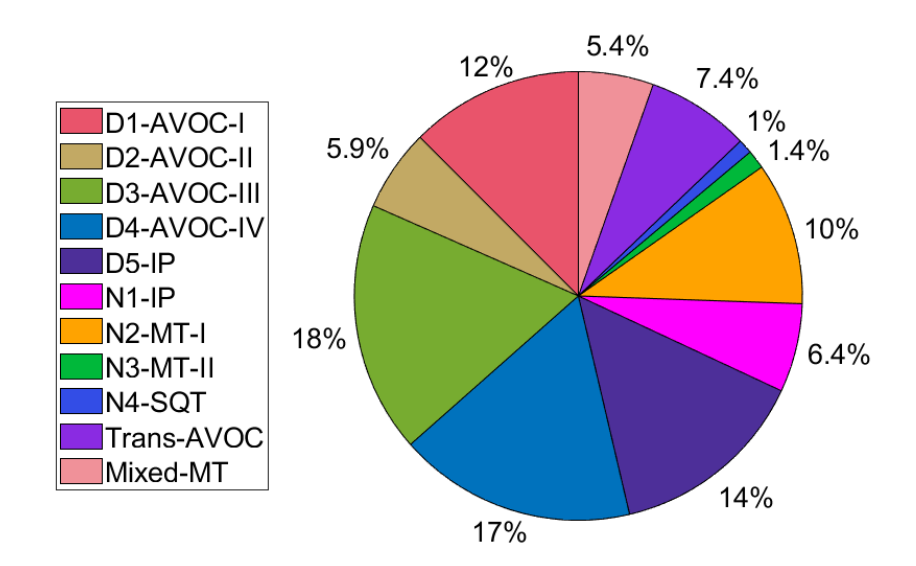


Figure S6. Relative contributions of the 11 factors to the total concentration of measured OOMs.

179 S6 Correlation of binPMF factors with other data

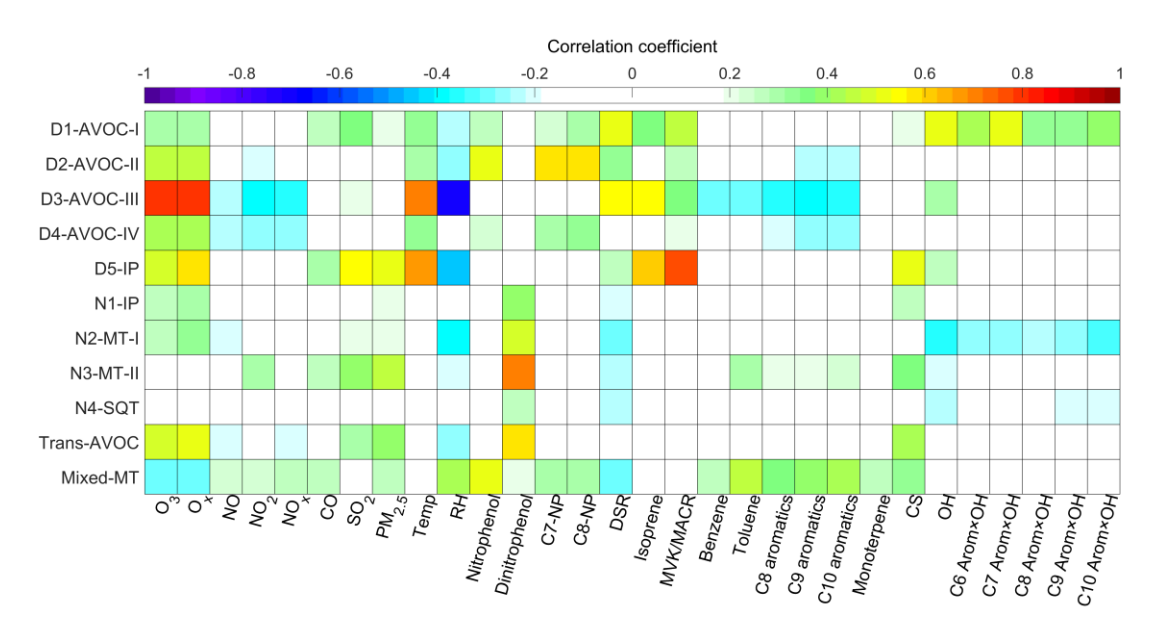


Figure S7. Correlations of factors with external gas-phase and particulate tracers. The colors are differentiated by Pearson correlation coefficients.

184 S7 Reactivity of nighttime oxidants with BVOCs

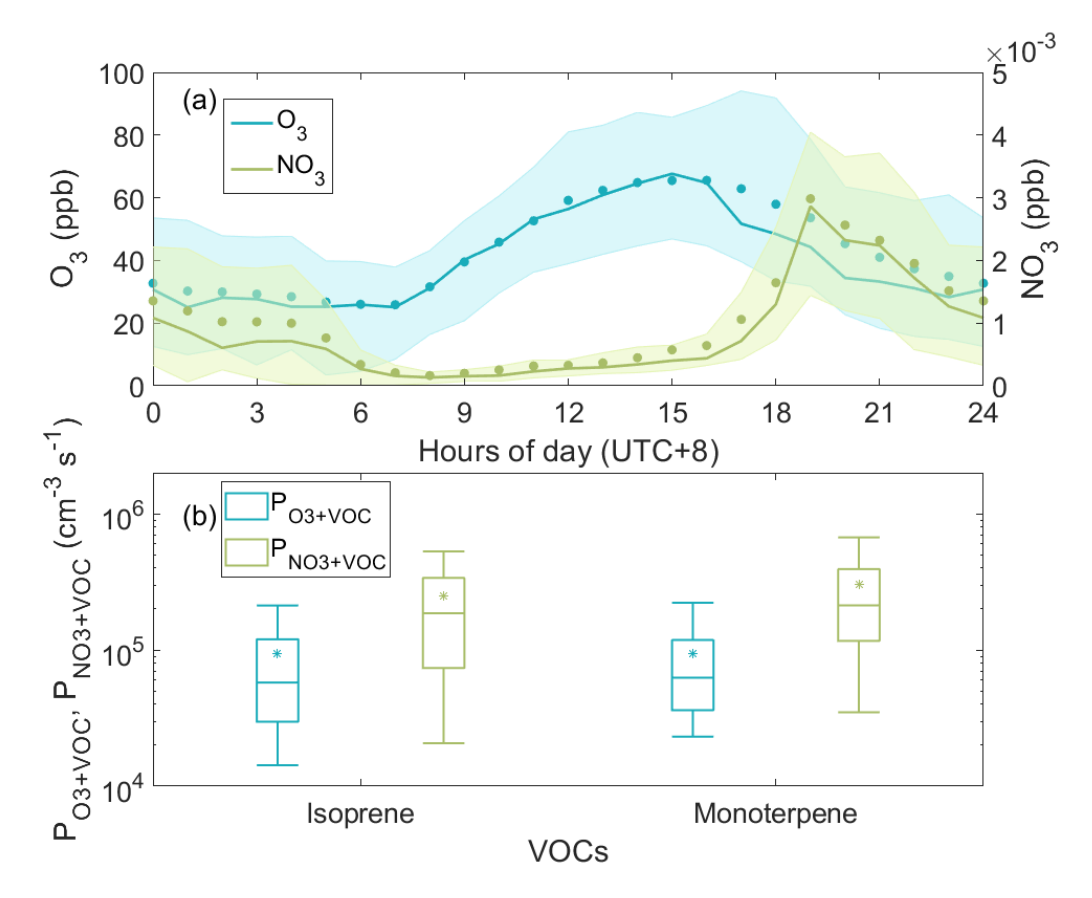


Figure S8. (a) Diurnal variations of O₃ and NO₃ radical. (b) Box plot of the oxidation reaction rates of isoprene and monoterpenes by O₃ and NO₃ radical at nighttime.

189 S8 Time series of N1-IP factor and C₅H₈O₅N

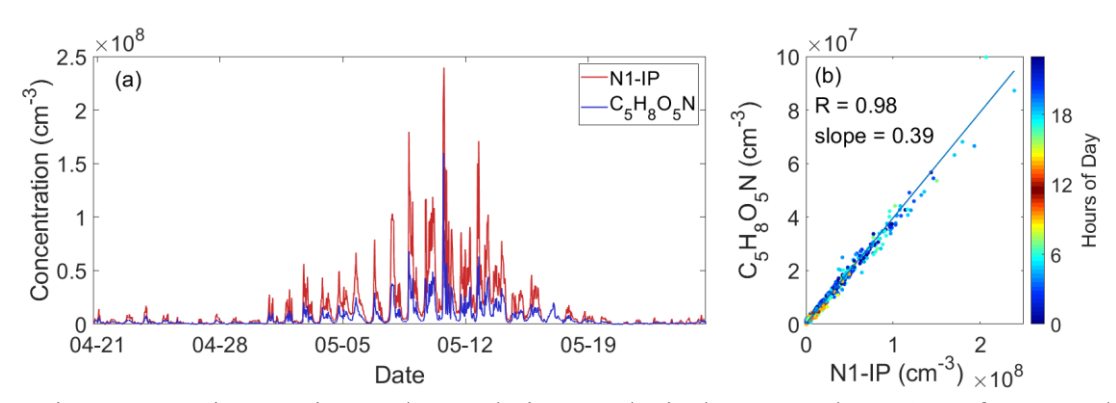


Figure S9. Time series and correlation analysis between the N1-IP factor and $C_5H_8O_5N$. (a) Temporal evolution of the N1-IP factor (red) and $C_5H_8O_5N$ (blue) obtained from direct peak fitting. (b) Correlation between $C_5H_8O_5N$ and the N1-IP factor, colored by hours of day.

S9 Dynamic chemical analysis of specific factors

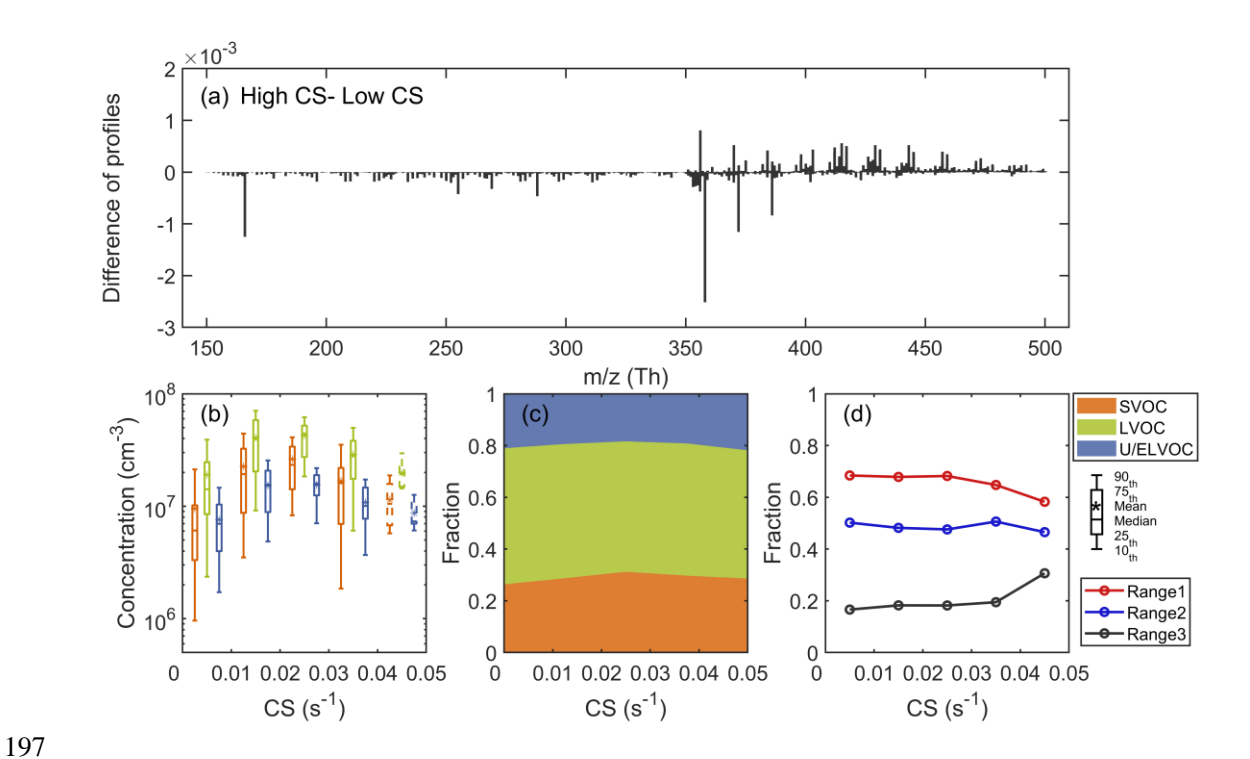


Figure S10. Characteristics of the D3-AVOC-III factor under varying condensation sink (CS) conditions. (a) Difference between the average mass spectra of D3-AVOC-III under high CS (above the upper quartile) and low CS (below the lower quartile) conditions. (b) Boxplots of the concentrations of SVOC, LVOC, and U/ELVOC species binned by CS in each $0.01~\rm s^{-1}$ interval. Data for CS > $0.04~\rm s^{-1}$ are represented by dashed box plots owing too few data points. (c) Fractional contributions of SVOC, LVOC, and U/ELVOC species across different CS conditions. (d) Evolution of fractional contributions of three sub-ranges as a function of CS.

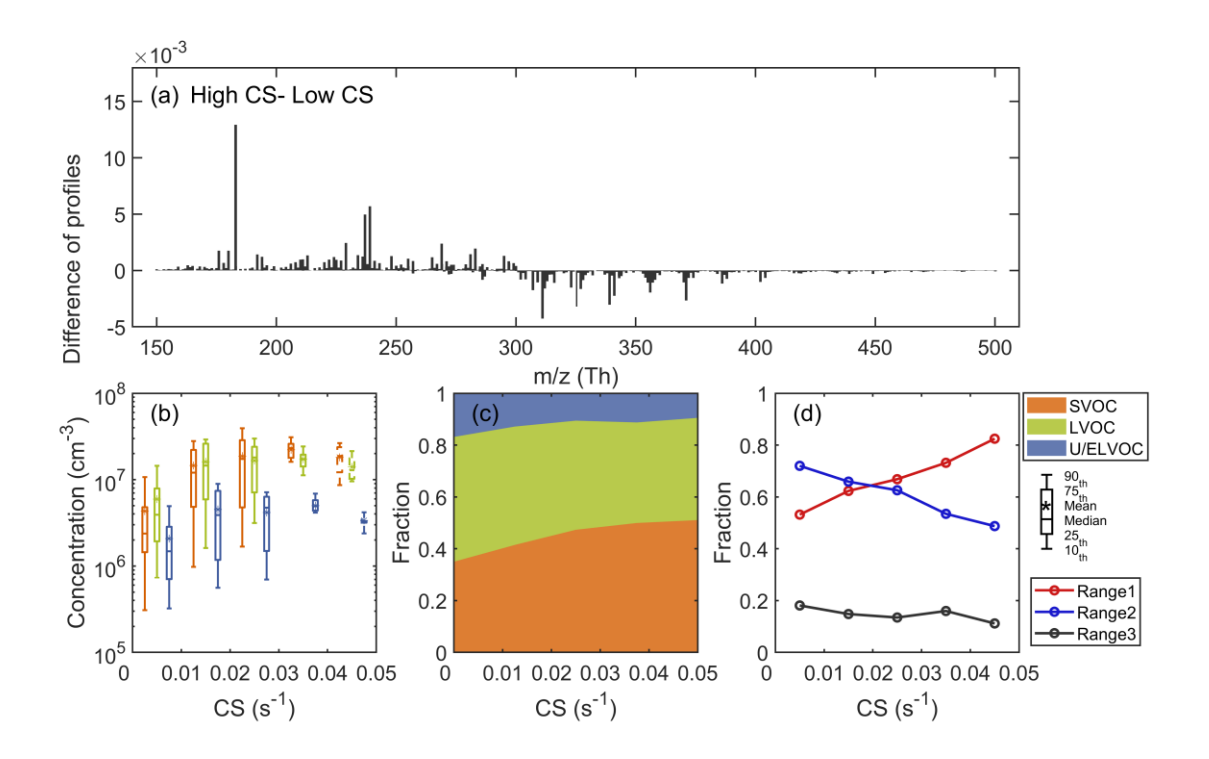


Figure S11. Characteristics of the N2-MT-I factor under varying condensation sink (CS) conditions. (a) Difference between the average mass spectra of N2-MT-I under high CS (above the upper quartile) and low CS (below the lower quartile) conditions. (b) Boxplots of the concentrations of SVOC, LVOC, and U/ELVOC species binned by CS in each $0.01~\rm s^{-1}$ interval. Data for CS > $0.04~\rm s^{-1}$ are represented by dashed box plots owing too few data points. (c) Fractional contributions of SVOC, LVOC, and U/ELVOC species across different CS conditions. (d) Evolution of fractional contributions of three sub-ranges as a function of CS.

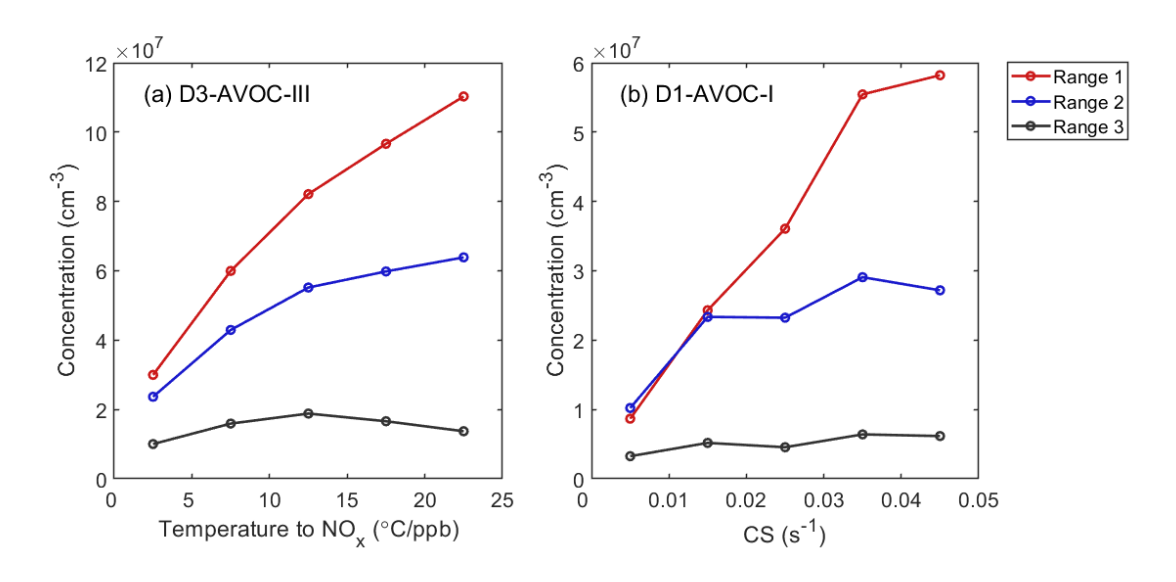


Figure S12. Evolution of concentrations of three sub-ranges of (a) D3-AVOC-III with T/NO_x ratio, and (b) D1-AVOC-I with CS.

S10 Main peaks of binPMF factors

Table S2. Molecular characteristics of D1-AVOC-I factor. The reagent ion has been omitted from the formulas.

Range	No.	Formulas	Contribution to the Range (%)	DBE	$n_{\rm O}$	$n_{\rm N}$
	1	$C_xH_{2x-1}O_6N, x = [3, 9]$	18.6	1	6	1
	2	$C_xH_{2x-2}O_4$, $x = [3, 10]$	9.6	2	4	0
R1	3	$C_xH_{2x-3}O_7N$, $x = [4, 8]$	8.3	2	7	1
	4	$C_xH_{2x-3}O_6N$, $x = [4, 9]$	6.7	2	6	1
	5	$C_xH_{2x-5}O_7N$, $x = [5, 8]$	5.1	3	7	1
	1	$C_xH_{2x-1}O_6N$, $x = [6, 13]$	13.1	1	6	1
	2	$C_xH_{2x-5}O_8N$, $x = [5, 14]$	9.9	3	8	1
R2	3	$C_xH_{2x-3}O_7N$, $x = [5, 15]$	8.8	2	7	1
	4	$C_xH_{2x-5}O_7N$, $x = [5, 14]$	7.5	3	7	1
	5	$C_xH_{2x-3}O_6N$, $x = [6, 14]$	6.1	2	6	1
	1	$C_xH_{2x-5}O_8N$, $x = [11, 18]$	4.3	3	8	1
	2	$C_xH_{2x-5}O_9N$, $x = [10, 17]$	3.5	3	9	1
R3	3	$C_xH_{2x-4}O_{10}N_2$, $x = [9, 16]$	3.3	2	10	2
	4	$C_xH_{2x-3}O_8N$, $x = [11, 18]$	3.0	2	8	1
	5	$C_xH_{2x-3}O_7N$, $x = [12, 18]$	2.8	2	7	1

Table S3. Molecular characteristics of D2-AVOC-II factor. The reagent ion has been omitted from the formulas.

Range	No.	Formulas	Contribution to the Range (%)	DBE	no	$n_{\rm N}$
	1	$C_xH_{2x-2}O_8N_2$, $x = [6, 13]$	14.8	1	8	2
	2	$C_xH_{2x-3}O_7N$, $x = [5, 14]$	9.3	2	7	1
R2	3	$C_xH_{2x-1}O_6N$, $x = [6, 14]$	9.3	1	6	1
	4	$C_xH_{2x-4}O_{10}N_2$, $x = [7, 11]$	6.7	2	10	2
	5	$C_xH_{2x}O_8N_2$, $x = [5, 13]$	6.5	0	8	2
	1	$C_xH_{2x-4}O_{10}N_2$, $x = [8, 12]$	18.3	2	10	2
	2	$C_xH_{2x-2}O_8N_2$, $x = [10, 18]$	12.3	1	8	2
R3	3	$C_xH_{2x}O_7N_2$, $x = [11, 19]$	8.5	0	7	2
	4	$C_xH_{2x-4}O_8N_2$, $x = [10, 17]$	6.2	2	8	2
	5	$C_xH_{2x}O_8N_2$, $x = [10, 15]$	4.1	0	8	2

Table S4. Molecular characteristics of D3-AVOC-III factor. The reagent ion has been omitted from the formulas.

Range	No.	Formulas	Contribution to the Range (%)	DBE	$n_{\rm O}$	$n_{\rm N}$
	1	$C_xH_{2x-2}O_4$, $x = [3]$	12.4	2	4	0
	2	$C_xH_{2x-3}O_7N$, $x = [4, 8]$	7.6	2	7	1
R1	3	$C_xH_{2x-4}O_5$, $x = [4, 10]$	7.3	3	5	0
	4	$C_xH_{2x-6}O_5$, $x = [5, 10]$	6.1	4	5	0
	5	$C_xH_{2x-2}O_5, x = [4, 9]$	6.0	2	5	0
	1	$C_xH_{2x-3}O_7N$, $x = [5, 11]$	11.1	2	7	1
	2	$C_xH_{2x-5}O_7N$, $x = [5, 11]$	6.1	3	7	1
R2	3	$C_xH_{2x-5}O_8N$, $x = [5, 12]$	6.1	3	8	1
	4	$C_xH_{2x-3}O_8N$, $x = [5, 11]$	6.0	2	8	1
	5	$C_xH_{2x}O_8N_2, x = [5]$	5.7	0	8	2
	1	$C_xH_{2x-4}O_{10}N_2$, $x = [8, 15]$	13.0	2	10	2
	2	$C_xH_{2x-4}O_9N_2$, $x = [9, 16]$	5.7	2	9	2
R3	3	$C_xH_{2x-2}O_9N_2$, $x = [9, 16]$	4.1	1	9	2
	4	$C_xH_{2x-2}O_8N_2$, $x = [10, 16]$	4.1	1	8	2
	5	$C_xH_{2x-1}O_{10}N_3, x = [7, 15]$	3.4	0	10	3

Table S5. Molecular characteristics of D4-AVOC-IV factor. The reagent ion has been omitted from the formulas.

Range	No.	Formulas	Contribution to the Range (%)	DBE	$n_{\rm O}$	$n_{\rm N}$
	1	$C_xH_{2x-2}O_4$, $x = [3, 9]$	16.8	2	4	0
	2	$C_xH_{2x-3}O_6N$, $x = [4, 9]$	15.4	2	6	1
R1	3	$C_xH_{2x-1}O_6N, x = [3, 9]$	15.2	1	6	1
	4	$C_xH_{2x-1}O_5N$, $x = [2, 5]$	9.1	1	5	1
	5	$C_xH_{2x-4}O_4$, $x = [5, 10]$	6.6	3	4	0
	1	$C_xH_{2x-1}O_6N, x = [6, 12]$	14.8	1	6	1
	2	$C_xH_{2x-3}O_6N$, $x = [6, 14]$	13.9	2	6	1
R2	3	$C_xH_{2x-3}O_7N$, $x = [5, 12]$	6.5	2	7	1
	4	$C_xH_{2x-2}O_8N_2$, $x = [4, 9]$	4.8	1	8	2
	5	$C_xH_{2x-5}O_7N$, $x = [7, 13]$	4.2	3	7	1

Table S6. Molecular characteristics of D5-IP factor. The reagent ion has been omitted from the formulas.

Range	No.	Formulas	Contribution to the Range (%)	DBE	$n_{\rm C}$	$n_{\rm N}$
	1	$C_5H_{10}O_xN_2, x = [8]$	45.7	0	5	2
	2	$C_5H_9O_xN, x = [4, 9]$	4.6	1	5	1
R1	3	$C_5H_8O_xN_2, x = [7, 8]$	3.8	1	5	2
	4	$C_4H_7O_xN, x = [5, 6]$	3.6	1	4	1
	5	$C_5H_7O_xN, x = [3, 8]$	3.4	2	5	1
	1	$C_5H_{10}O_xN_2, x = [8, 9]$	45.4	0	5	2
	2	$C_5H_9O_xN_3$, $x = [10, 11]$	6.9	0	5	3
R2	3	$C_5H_8O_xN_2, x = [8, 9]$	4.0	1	5	2
	4	$C_6H_{10}O_xN_2, x = [8, 9]$	1.8	1	6	2
	5	$C_7H_{10}O_xN_2$, $x = [8, 10]$	1.6	2	7	2
	1	$C_{10}H_{16}O_xN_2, x = [8, 14]$	5.6	2	10	2
	2	$C_5H_{10}O_xN_2, x = [8]$	5.6	0	5	2
R3	3	$C_{10}H_{17}O_xN_3, x = [10, 14]$	4.3	1	10	3
	4	$C_9H_{14}O_xN_2$, $x = [9, 14]$	3.9	2	9	2
	5	$C_5H_9O_xN_3, x = [10]$	3.1	0	5	3

Table S7. Molecular characteristics of N1-IP factor. The reagent ion has been omitted from the formulas.

Range	No.	Formulas	Contribution to the Range (%)	DBE	$n_{\rm C}$	$n_{\rm N}$
	1	$C_5H_8O_xN\cdot, x=[5]$	57.4	1.5	5	1
	2	$C_6H_{10}O_x, x = [5]$	8.7	2	6	0
R3	3	$C_6H_{11}O_xN$, $x = [6, 8]$	3.8	1	6	1
	4	$C_5H_9O_xN, x = [5, 6]$	2.9	1	5	1
	5	$C_7H_9O_xN, x = [6, 8]$	2.6	3	7	1

Table S8. Molecular characteristics of N2-MT-I factor. The reagent ion has been omitted from the formulas.

Range	No.	Formulas	Contribution to the Range (%)	DBE	$n_{\rm C}$	$n_{\rm N}$
	1	$C_7H_9O_xN, x = [6, 8]$	8.5	3	7	1
	2	$C_2H_3O_xN, x = [5]$	7.0	1	2	1
R1	3	$C_7H_{11}O_xN$, $x = [6, 8]$	6.8	2	7	1
	4	$C_6H_9O_xN, x = [5, 8]$	6.4	2	6	1
	5	$C_5H_7O_xN, x = [5, 8]$	5.1	2	5	1
	1	$C_7H_9O_xN, x = [6, 9]$	6.7	3	7	1
	2	$C_{10}H_{15}O_xN$, $x = [6, 10]$	6.6	3	10	1
R2	3	$C_9H_{15}O_xN$, $x = [6, 9]$	6.2	2	9	1
	4	$C_{10}H_{17}O_xN$, $x = [6, 10]$	5.5	2	10	1
	5	$C_6H_{11}O_xN$, $x = [6, 9]$	5.1	1	6	1
	1	$C_{10}H_{15}O_xN$, $x = [9, 12]$	9.0	3	10	1
	2	$C_{10}H_{16}O_xN_2$, $x = [8, 13]$	6.3	2	10	2
R3	3	$C_{10}H_{16}O_xN\cdot, x = [9, 11]$	6.1	2.5	10	1
	4	$C_{10}H_{18}O_xN_2$, $x = [8, 12]$	5.1	1	10	2
	5	$C_9H_{16}O_xN_2$, $x = [9, 13]$	4.0	1	9	2

Table S9. Molecular characteristics of N3-MT-II factor. The reagent ion has been omitted from the formulas.

Range	No.	Formulas	Contribution to the Range (%)	DBE	$n_{\rm C}$	$n_{\rm N}$
	1	$C_{10}H_{16}O_xN_2, x = [8, 13]$	17.7	2	10	2
	2	$C_{10}H_{18}O_xN_2$, $x = [8, 13]$	16.7	1	10	2
R3	3	$C_{10}H_{17}O_xN_3$, $x = [10, 13]$	7.4	1	10	3
	4	$C_{10}H_{16}O_xN\cdot, x = [9, 11]$	3.0	2.5	10	1
	5	$C_9H_{16}O_xN_2$, $x = [9, 13]$	2.9	1	9	2

Table S10. Molecular characteristics of N4-SQT factor. The reagent ion has been omitted from the formulas.

Range	No.	Formulas	Contribution to the Range (%)	DBE	$n_{\rm C}$	$n_{\rm N}$
	1	$C_{15}H_{23}O_xN$, $x = [6, 12]$	14.3	4	15	1
	2	$C_{15}H_{24}O_xN\cdot, x = [7, 13]$	7.6	3.5	15	1
R3	3	$C_{15}H_{25}O_xN$, $x = [6, 13]$	5.8	3	15	1
	4	$C_{15}H_{24}O_xN_2$, $x = [8, 12]$	5.3	3	15	2
	5	$C_{11}H_{16}O_xN_2$, $x = [9, 13]$	3.9	3	11	2

Table S11. Molecular characteristics of Trans-AVOC factor. The reagent ion has been omitted from the formulas.

Range	No.	Formulas	Contribution to the Range (%)	DBE	$n_{\rm O}$	$n_{\rm N}$
	1	$C_xH_{2x-2}O_8N_2$, $x = [4, 12]$	20.2	1	8	2
	2	$C_xH_{2x-3}O_6N$, $x = [6, 11]$	18.0	2	6	1
R2	3	$C_xH_{2x-1}O_6N$, $x = [6, 10]$	10.4	1	6	1
	4	$C_xH_{2x-3}O_{10}N$, $x = [5, 11]$	5.6	2	10	1
	5	$C_xH_{2x}O_7N_2$, $x = [5, 11]$	4.5	0	7	2
	1	$C_xH_{2x-3}O_{10}N_3, x = [7, 14]$	11.0	1	10	3
	2	$C_xH_{2x-1}O_{10}N_3, x = [7, 13]$	8.0	0	10	3
R3	3	$C_xH_{2x-3}O_{11}N_3, x = [6, 14]$	7.6	1	11	3
	4	$C_xH_{2x-2}O_8N_2$, $x = [10, 14]$	7.2	1	8	2
	5	$C_xH_{2x-4}O_9N_2$, $x = [9, 14]$	5.2	2	9	2

264

Table S12. Molecular characteristics of Mixed-MT factor. The reagent ion has been omitted from the formulas.

Range	No.	Formulas	Contribution to the Range (%)	DBE	$n_{\rm O}$	$n_{\rm N}$
R2	1	$C_xH_{2x-3}O_6N$, $x = [6, 14]$	10.2	2	6	1
	2	$C_xH_{2x-5}O_6N$, $x = [6, 15]$	7.2	3	6	1
	3	$C_xH_{2x-1}O_6N$, $x = [6, 12]$	6.6	1	6	1
	4	$C_xH_{2x}O_7N_2$, $x = [5, 14]$	6.0	0	7	2
	5	$C_xH_{2x-1}O_5N$, $x = [7, 13]$	5.0	1	5	1
R3	1	$C_xH_{2x-2}O_8N_2$, $x = [10, 15]$	9.3	1	8	2
	2	$C_xH_{2x-4}O_8N_2$, $x = [10, 15]$	7.9	2	8	2
	3	$C_xH_{2x-4}O_9N_2$, $x = [9, 15]$	5.9	2	9	2
	4	$C_xH_{2x}O_7N_2$, $x = [11, 16]$	5.4	0	7	2
	5	$C_xH_{2x-3}O_{10}N_3$, $x = [7, 13]$	3.2	1	10	3

265266

267

268

Reference:

- Donahue, N. M., Epstein, S. A., Pandis, S. N., and Robinson, A. L.: A two-dimensional volatility basis set: 1. organic-aerosol mixing thermodynamics, Atmos Chem Phys, 2011.
- Epstein, S. A., Riipinen, I., and Donahue, N. M.: A Semiempirical Correlation between Enthalpy of
- Vaporization and Saturation Concentration for Organic Aerosol, Environ. Sci. Technol., 44, 743–
- 273 748, https://doi.org/10.1021/es902497z, 2010.
- Finlayson-Pitts, B. J. and Pitts, J. N.: Acid Deposition Formation and Fates of Inorganic and Organic
- Acids in the Troposphere, in: Chemistry of the Upper and Lower Atmosphere, vol. 8, Academic
- 276 Press, 294–348, 2000.

- Fuchs, N. A. and Sutugin, A. G.: HIGH-DISPERSED AEROSOLS, in: Topics in Current Aerosol
- 278 Research, Elsevier, 1, https://doi.org/10.1016/B978-0-08-016674-2.50007-8, 1971.
- 279 Kroll, J. H., Donahue, N. M., Jimenez, J. L., Kessler, S. H., Canagaratna, M. R., Wilson, K. R.,
- Altieri, K. E., Mazzoleni, L. R., Wozniak, A. S., Bluhm, H., Mysak, E. R., Smith, J. D., Kolb, C. E.,
- and Worsnop, D. R.: Carbon oxidation state as a metric for describing the chemistry of atmospheric
- organic aerosol, Nat. Chem., 3, 133–139, https://doi.org/10.1038/nchem.948, 2011.
- Kulmala, M., Petäjä, T., Nieminen, T., Sipilä, M., Manninen, H. E., Lehtipalo, K., Dal Maso, M.,
- Aalto, P. P., Junninen, H., Paasonen, P., Riipinen, I., Lehtinen, K. E. J., Laaksonen, A., and Kerminen,
- V.-M.: Measurement of the nucleation of atmospheric aerosol particles, Nat. Protoc., 7, 1651–1667,
- 286 https://doi.org/10.1038/nprot.2012.091, 2012.
- 287 Kürten, A., Rondo, L., Ehrhart, S., and Curtius, J.: Calibration of a Chemical Ionization Mass
- Spectrometer for the Measurement of Gaseous Sulfuric Acid, J. Phys. Chem. A, 116, 6375–6386,
- 289 https://doi.org/10.1021/jp212123n, 2012.
- 290 Liu, Y., Nie, W., Li, Y., Ge, D., Liu, C., Xu, Z., Chen, L., Wang, T., Wang, L., Sun, P., Qi, X., Wang,
- J., Xu, Z., Yuan, J., Yan, C., Zhang, Y., Huang, D., Wang, Z., Donahue, N. M., Worsnop, D., Chi,
- 292 X., Ehn, M., and Ding, A.: Formation of condensable organic vapors from anthropogenic and
- 293 biogenic volatile organic compounds (VOCs) is strongly perturbed by NOx in eastern China,
- 294 Atmospheric Chem. Phys., 21, 14789–14814, https://doi.org/10.5194/acp-21-14789-2021, 2021.
- 295 Liu, Y., Liu, C., Nie, W., Li, Y., Ge, D., Chen, L., Zhu, C., Wang, L., Zhang, Y., Liu, T., Qi, X., Wang,
- J., Huang, D., Wang, Z., Yan, C., Chi, X., and Ding, A.: Exploring condensable organic vapors and
- their co-occurrence with PM _{2.5} and O ₃ in winter in Eastern China, Environ. Sci. Atmospheres, 3,
- 298 282–297, https://doi.org/10.1039/D2EA00143H, 2023.
- 299 Mohr, C., Thornton, J. A., Heitto, A., Lopez-Hilfiker, F. D., Lutz, A., Riipinen, I., Hong, J., Donahue,
- N. M., Hallquist, M., Petäjä, T., Kulmala, M., and Yli-Juuti, T.: Molecular identification of organic
- 301 vapors driving atmospheric nanoparticle growth, Nat. Commun., 10, 4442,
- 302 https://doi.org/10.1038/s41467-019-12473-2, 2019.
- 303 Nie, W., Yan, C., Huang, D. D., Wang, Z., Liu, Y., Qiao, X., Guo, Y., Tian, L., Zheng, P., Xu, Z., Li,
- Y., Xu, Z., Qi, X., Sun, P., Wang, J., Zheng, F., Li, X., Yin, R., Dallenbach, K. R., Bianchi, F., Petäjä,
- T., Zhang, Y., Wang, M., Schervish, M., Wang, S., Qiao, L., Wang, Q., Zhou, M., Wang, H., Yu, C.,
- 306 Yao, D., Guo, H., Ye, P., Lee, S., Li, Y. J., Liu, Y., Chi, X., Kerminen, V.-M., Ehn, M., Donahue, N.
- 307 M., Wang, T., Huang, C., Kulmala, M., Worsnop, D., Jiang, J., and Ding, A.: Secondary organic
- aerosol formed by condensing anthropogenic vapours over China's megacities, Nat. Geosci., 15,
- 309 255–261, https://doi.org/10.1038/s41561-022-00922-5, 2022.
- 310 Stolzenburg, D., Fischer, L., Vogel, A. L., Heinritzi, M., Schervish, M., Simon, M., Wagner, A. C.,
- Dada, L., Ahonen, L. R., Amorim, A., Baccarini, A., Bauer, P. S., Baumgartner, B., Bergen, A.,
- 312 Bianchi, F., Breitenlechner, M., Brilke, S., Buenrostro Mazon, S., Chen, D., Dias, A., Draper, D. C.,
- Duplissy, J., El Haddad, I., Finkenzeller, H., Frege, C., Fuchs, C., Garmash, O., Gordon, H., He, X.,
- Helm, J., Hofbauer, V., Hoyle, C. R., Kim, C., Kirkby, J., Kontkanen, J., Kürten, A., Lampilahti, J.,

- Lawler, M., Lehtipalo, K., Leiminger, M., Mai, H., Mathot, S., Mentler, B., Molteni, U., Nie, W.,
- Nieminen, T., Nowak, J. B., Ojdanic, A., Onnela, A., Passananti, M., Petäjä, T., Quéléver, L. L. J.,
- Rissanen, M. P., Sarnela, N., Schallhart, S., Tauber, C., Tomé, A., Wagner, R., Wang, M., Weitz, L.,
- Wimmer, D., Xiao, M., Yan, C., Ye, P., Zha, Q., Baltensperger, U., Curtius, J., Dommen, J., Flagan,
- 319 R. C., Kulmala, M., Smith, J. N., Worsnop, D. R., Hansel, A., Donahue, N. M., and Winkler, P. M.:
- Rapid growth of organic aerosol nanoparticles over a wide tropospheric temperature range, Proc.
- 321 Natl. Acad. Sci., 115, 9122–9127, https://doi.org/10.1073/pnas.1807604115, 2018.
- 322 Ulbrich, I. M., Canagaratna, M. R., Zhang, Q., Worsnop, D. R., and Jimenez, J. L.: Interpretation of
- 323 organic components from Positive Matrix Factorization of aerosol mass spectrometric data, Atmos
- 324 Chem Phys, 2009.
- Yan, C., Nie, W., Äijälä, M., Rissanen, M. P., Canagaratna, M. R., Massoli, P., Junninen, H., Jokinen,
- 326 T., Sarnela, N., Häme, S. A. K., Schobesberger, S., Canonaco, F., Yao, L., Prévôt, A. S. H., Petäjä,
- 327 T., Kulmala, M., Sipilä, M., Worsnop, D. R., and Ehn, M.: Source characterization of highly
- 328 oxidized multifunctional compounds in a boreal forest environment using positive matrix
- 329 factorization, Atmospheric Chem. Phys., 16, 12715–12731, https://doi.org/10.5194/acp-16-12715-
- 330 2016, 2016.

- Zhang, Y., Peräkylä, O., Yan, C., Heikkinen, L., Äijälä, M., Daellenbach, K. R., Zha, Q., Riva, M.,
- 332 Garmash, O., Junninen, H., Paatero, P., Worsnop, D., and Ehn, M.: A novel approach for simple
- statistical analysis of high-resolution mass spectra, Atmospheric Meas. Tech., 12, 3761–3776,
- 334 https://doi.org/10.5194/amt-12-3761-2019, 2019.